



Analytical analysis and implementation of a low-speed high-torque permanent magnet vernier in-wheel motor for electric vehicle

Jianguo Li, Junhua Wang, Zhao Zhigang, and Weili Yan

Citation: *J. Appl. Phys.* **111**, 07E727 (2012); doi: 10.1063/1.3677878

View online: <http://dx.doi.org/10.1063/1.3677878>

View Table of Contents: <http://jap.aip.org/resource/1/JAPIAU/v111/i7>

Published by the [American Institute of Physics](#).

Related Articles

Permanent magnet online magnetization performance analysis of a flux mnemonic double salient motor using an improved hysteresis model

J. Appl. Phys. **111**, 07D119 (2012)

Design and analysis of new fault-tolerant permanent magnet motors for four-wheel-driving electric vehicles

J. Appl. Phys. **111**, 07E713 (2012)

Design of a spoke-type permanent-magnet motor with optimal winding configuration for electric vehicle applications

J. Appl. Phys. **111**, 07E710 (2012)

Field weakening capability investigation of an axial flux permanent-magnet synchronous machine with radially sliding permanent magnets used for electric vehicles

J. Appl. Phys. **111**, 07A719 (2012)

Power management strategy based on adaptive neuro-fuzzy inference system for fuel cell-battery hybrid vehicle

J. Renewable Sustainable Energy **4**, 013106 (2012)

Additional information on *J. Appl. Phys.*

Journal Homepage: <http://jap.aip.org/>

Journal Information: http://jap.aip.org/about/about_the_journal

Top downloads: http://jap.aip.org/features/most_downloaded

Information for Authors: <http://jap.aip.org/authors>

ADVERTISEMENT



**FIND THE NEEDLE IN THE
HIRING HAYSTACK**

Post jobs and reach
thousands of hard-to-find
scientists with specific skills



<http://careers.physicstoday.org/post.cfm> **physicstoday JOBS**

Analytical analysis and implementation of a low-speed high-torque permanent magnet vernier in-wheel motor for electric vehicle

Jiangui Li,^{1,a)} Junhua Wang,² Zhao Zhigang,³ and Weili Yan³

¹Department of Electrical and Electronic Engineering, The University of Hong Kong, Hong Kong

²Department of Electrical Engineering, The Hong Kong Polytechnic University, Kowloon, Hong Kong

³Joint Key Laboratory of EFEAR, Hebei University of Technology, Tianjin 300130, China

(Presented 31 October 2011; received 23 September 2011; accepted 22 November 2011; published online 8 March 2012)

In this paper, analytical analysis of the permanent magnet vernier (PMV) is presented. The key is to analytically solve the governing Laplacian/quasi-Poissonian field equations in the motor regions. By using the time-stepping finite element method, the analytical method is verified. Hence, the performances of the PMV machine are quantitatively compared with that of the analytical results. The analytical results agree well with the finite element method results. Finally, the experimental results are given to further show the validity of the analysis. © 2012 American Institute of Physics. [doi:10.1063/1.3677878]

The permanent magnet vernier (PMV) machines are becoming promising candidate for low-speed applications, such as direct-drive wind power generation. However, the theory analysis of PMV machine is mainly based on magnetic circuit method in which only the fundamental component is considered.^{1,2} The intrinsic principle of PMV machine need to be further studied to provide physical insight for the designer. Although some viable analytical methods have been proposed for magnetic gears³ and slotless PM machines,⁴ they generally do not contain the stator slot structure, which makes the problem much more difficult. The introductions of the flux-modulation-poles (FMPs) and stator slots in PMV machine make the problem complicated and difficult to solve. Although more accurate analytical methods have been developed for the PM machines,^{5,6} the PMV machine has not been proposed.

In this paper, the performances of the PMV motor are analyzed by analytical method while both of the stator slots and FMPs have been taken into consideration. The derivations of the induced voltage and torque have been presented and the results are verified by finite element methods. The analytical results agree well with the FEM results, which prove the viability of the method.

The configuration of a newly developed PMV machine is shown in Fig. 1. There are 6 slots in the inner stator, which are occupied by 3-phase armature windings. Each stator tooth of the PMV machine is split into 4 FMPs, which functions to modulate the high-frequency rotating PM filed of the outer rotor. Thus, it can offer low-speed operation for direct-drive applications. The corresponding relationship is governed by $p_r = N_s - p_s$, where N_s is the number of FMPs in the stator, p_r is the number of PM pole-pairs in the rotor and p_s is the number of armature winding pole-pairs in the stator.

The output torque relies on the interaction between the magnetic fields generated by the PMs and the armature windings. The magnetic flux density generated by the PMs is given by

$$B_{PM}(\theta_1) \approx (-1)^j \frac{1}{2} F_{PM1} P_1 \cos[(N_s - p_r)\theta_1 + p_r \theta_m] + F_{PM1} P_0 \cos[p_r(\theta_1 - \theta_m)], \quad (1)$$

where B_{PM} is the airgap flux density generated by the PMs; F_{PM1} is the amplitude of the fundamental component of PM magnetomotive force; P is the permeance of the magnetic path; θ_1 , θ_2 , θ_m are the initial mechanical angle on the stator, on the rotor and the rotor position, respectively.

Considering only the components of the magnetomotive force F_c generated by the armature windings that have the same orders as the terms in B_{PM} ; otherwise, they do not affect the net torque, it yields:

$$F_c \approx \frac{3}{2} k_{d1} k_{p1} F_{c1} \left\{ \cos[p_s \theta_1 - (\omega t - \alpha)] + (-1)^j p \cos[(N_s - p_s)\theta_1 + (\omega t - \alpha)] / (N_s - p_s) + (-1)^{j-1} p \cos[(N_s + p_s)\theta_1 - (\omega t - \alpha)] / (N_s + p_s) \right\}, \quad (2)$$

where $N_s \neq p_s$; and k_{d1} , k_{p1} are the distribution factor and the pitch factor of the fundamental component, respectively. From Eqs. (1) and (2), it can be found that the first and second term of Eq. (1) are the same if p_r is $N_s + p_s$, while they become opposite when $p_r = N_s - p_s$. To maximize the output torque, the PMV motor needs to adopt the relationship $p_r = N_s - p_s$.

In order to perform the analytical formulation for harmonic analysis, there are some basic assumptions: the permeability of both stator and rotor cores are infinite; the relative recoil permeability of PM equals to 1, and the end-effects are neglected. Firstly, the machine model without considering the FMPs is analyzed. Secondly, the model with FMPs is

^{a)}Present address: College of Electrical and Computer Science, University of Michigan, Dearborn, MI 48185, USA. Electronic mail: jgli@eee.hku.hk.

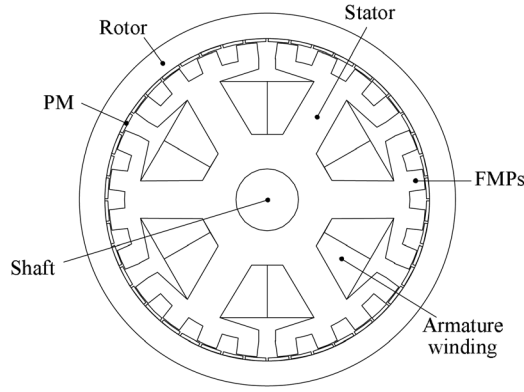


FIG. 1. Configuration of PMV machine.

analyzed. Meanwhile, the magnetic scalar potential is adopted to analyze the magnetic field of the machine.

The corresponding vector potential distribution in the PM subdomain I is governed by the Poisson's equation, while that in the airgap subdomain II is by the Laplace's equation. By applying the boundary conditions and the radial magnetization function, the airgap flux density can be deduced.^{5,6}

The modulation effect of the FMPs can be described by using the concept of complex relative airgap permeance. The permeance parameters are calculated by using the Schwarz–Christoffel transformation in such a way that the slotted structure can be transformed from the original plane to a new plane in which the structure becomes smooth. So, the analytical expression of magnetic flux density in the airgap is given by

$$B_M = B_o \lambda^*, \quad (3)$$

where B_M and B_o are the airgap flux densities with and without the FMPs, respectively, and λ^* is the complex relative airgap permeance. In polar coordinates, they can be written as

$$B_M = B_{rIFMPs} \vec{e}_r + B_{r\theta FMPs} \vec{e}_\theta, \quad B_o = B_{rII} \vec{e}_r + B_{r\theta II} \vec{e}_\theta, \quad (4)$$

$$\lambda^* = \lambda_a \vec{e}_r - \lambda_b \vec{e}_\theta, \quad (5)$$

$$\lambda_a = \lambda_0 + \sum_{k=1}^{\infty} \lambda_{ak} \cos(kN_s \theta), \quad \lambda_b = \sum_{k=1}^{\infty} \lambda_{bk} \sin(kN_s \theta), \quad (6)$$

where λ_0 , λ_{ak} , λ_{bk} are the Fourier coefficients.

The electromagnetic torque T_e is generated by the interaction of the magnetic field generated by the PMs and the armature currents. It can readily be deduced by using the Maxwell stress tensor and then the analytical expression of the electromagnetic torque becomes

$$T_e = \frac{\pi L R_e^2}{\mu_0} \sum_{n=1}^{\infty} (W_n X_n + Y_n Z_n), \quad (7)$$

where W_n , X_n , Y_n , and Z_n , are the Fourier expansions that can readily be determined using the boundary conditions

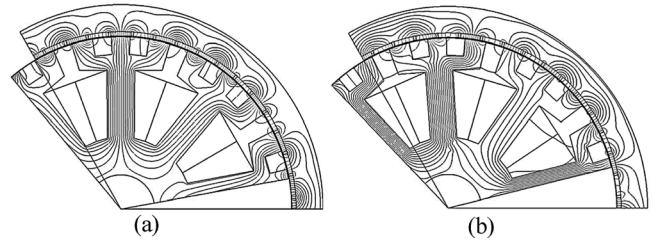


FIG. 2. Magnetic field distributions. (a) PMV machine at 0°. (b) PMV machine at 90°.

$$W_n = -A_n^{II} \frac{R_2 P_n(R_e, R_3)}{R_e E_n(R_2, R_3)} - B_n^{II} \frac{R_3 P_n(R_e, R_2)}{R_e E_n(R_3, R_2)},$$

$$X_n = -C_n^{II} \frac{R_2 E_n(R_e, R_3)}{R_e E_n(R_2, R_3)} - D_n^{II} \frac{R_3 P_n(R_e, R_2)}{R_e E_n(R_3, R_2)}, \quad (8)$$

$$Y_n = C_n^{II} \frac{R_2 P_n(R_e, R_3)}{R_e E_n(R_2, R_3)} + D_n^{II} \frac{R_3 P_n(R_e, R_2)}{R_e E_n(R_3, R_2)},$$

$$Z_n = -A_n^{II} \frac{R_2 P_n(R_e, R_3)}{R_e E_n(R_2, R_3)} - B_n^{II} \frac{R_3 E_n(R_e, R_2)}{R_e E_n(R_3, R_2)},$$

where A_n^{II} , B_n^{II} , C_n^{II} , and D_n^{II} can readily be determined by

$$A_n^{II} = \frac{2}{2\pi} \int_0^{2\pi} \left. \frac{\partial A_I}{\partial r} \right|_{R_2} \cdot \cos(n\theta) \cdot d\theta, \quad (9)$$

$$B_n^{II} = \frac{2}{2\pi} \int_0^{2\pi} f(\theta) \cdot \cos(n\theta) \cdot d\theta,$$

$$C_n^{II} = \frac{2}{2\pi} \int_0^{2\pi} \left. \frac{\partial A_I}{\partial r} \right|_{R_2} \cdot \sin(n\theta) \cdot d\theta,$$

$$D_n^{II} = \frac{2}{2\pi} \int_0^{2\pi} f(\theta) \cdot \sin(n\theta) \cdot d\theta,$$

$$f(\theta) = \begin{cases} \left. \frac{\partial A_i}{\partial r} \right|_{r=R_3}, & \forall \theta \in \text{slot opening}, \\ 0, & \text{else}, \end{cases} \quad (10)$$

where A_i is the vector potential in i_{th} slot opening, P_n and E_n is defined by

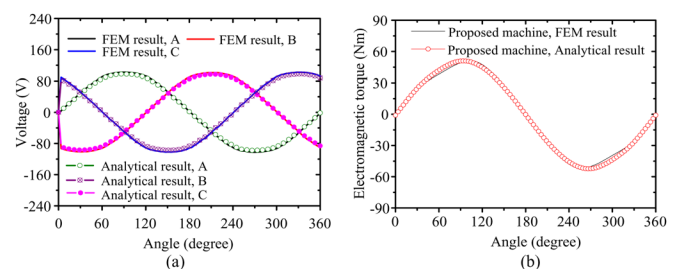


FIG. 3. (Color online) PMV machine characteristics. (a) No-load EMF. (b) Electromagnetic torque.

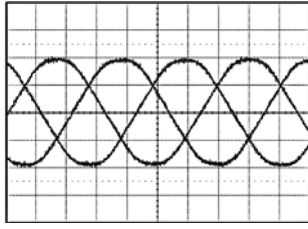


FIG. 4. Measured no-load EMF waveforms of PMV machine (50 V/div, 2 ms/div).

$$P_n(a, b) = \left(\frac{a}{b}\right)^n + \left(\frac{b}{a}\right)^n, \quad (11)$$

$$E_n(a, b) = \left(\frac{a}{b}\right)^n - \left(\frac{b}{a}\right)^n.$$

In order to compute the no-load EMF of a three-phase machine, the first step is to calculate the magnetic scalar potential of each slot j at a given rotor position. Considering that the current density is uniformly distributed over the slot area, the magnetic scalar potential can be averaged over the slot area to represent the coil as

$$\varphi_j = \frac{L}{S_{slot}} \iint_{S_{slot}} A_j(r, \theta) r \cdot dr \cdot d\theta. \quad (12)$$

Hence, the three-phase flux vector can be expressed as

$$(\psi_a \ \psi_b \ \psi_c)' = n_{turn} \cdot [C] \cdot (\varphi_1 \varphi_2 \cdots \varphi_{2Q-1} \varphi_{2Q})', \quad (13)$$

where n_{turn} is the number of turns in series per phase and $[C]$ is a connecting matrix that represents the stator winding distribution in the slots. Consequently, at a given position Δ , the three-phase no-load EMF vector is represented by

$$(E_a \ E_b \ E_c)' = \Omega \cdot \frac{d}{d\Delta} \cdot (\psi_a \ \psi_b \ \psi_c)'. \quad (14)$$

Firstly, the FEM is applied to analyze the magnetic field distributions of the PMV machine under no-load at two extreme rotor positions, namely at 0° and 90° electrical degree, as shown in Fig. 2. It can be observed that the magnetic field rotates 90° electrical degree while the rotor rotates only 3.75° mechanical degree. This indicates that this machine can provide low-speed high-torque operation. It also can be observed that the flux lines per stator tooth of the PMV machine can pass through the FMPs separately, hence verifying the desired flux modulation in both machines.

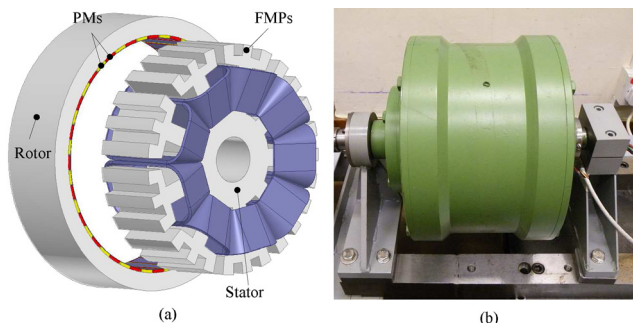


FIG. 5. (Color online) Prototype of the proposed PMV motor. (a) Scheme. (b) Photo.

TABLE I. Key design data.

Rated power	2 kW
Rated speed	200 rpm
No. of phases	3
No. of stator pole-pairs	3
No. of stator slots	27
No. of rotor pole-pairs	48
Overall outside diameter	240 mm
Shaft diameter	40 mm
Axial length	60 mm
Airgap length	0.6 mm

Secondly, the radial airgap flux density waveform and its harmonic spectra are simulated by using both the proposed analytical calculation and the FEM. The radial airgap flux density has been analyzed and the 3rd, 24th, 48th, 72nd, and 120th harmonics have prominent values due to the slotting effect. Quantitatively, the averaged values of the radial component are 0.67 T.

Thirdly, Fig. 3(a) shows the no-load EMF waveforms of the PMV machine, obtained by both the analytical calculation and the FEM. As expected, the analytical results agree well with the FEM results. It can be found that the RMS values of the analytical results and simulation results are 65.9 and 69.8 V, respectively. Namely, the analytical result is 5.9% lower than the simulation result, which is acceptable.

Fourth, Fig. 3(b) shows the electromagnetic torque waveforms of PMV machine obtained by both the analytical calculation and the FEM. Again, as expected, the analytical results agree well with the FEM results. It can be found that the peak torques of the analytical result and the simulation result are 52.7 and 51.1 Nm, respectively. Namely, the analytical result of the PMV machine is 3.0% higher than FEM simulation result.

Finally, Fig. 4 shows the measured no-load EMF of the PMV machine. It can be found that the analytical and FEM results agree well with the experimental results. Thus, the proposed analytical method and FEM simulation for the design of PMV machine are verified, hence the validity for the PMV machine. The final system of the PMV machine is prototyped and tested under the same conditions as the analysis, shown in Fig. 5. Table I is the key design data of the final system.

In this paper, an analytical analysis of the PMV machine has been proposed and implemented. The key is to analytically solve the governing Laplacian/quasi-Poissonian field equations in the airgap regions. The analytical analysis results are quantitatively compared with that of the simulation results, showing that the analytical result of no-load EMF is 5.9% lower and torque is 3.0% higher than the simulation results which are acceptable. Finally, the experimental results verify the validity of the analytical analysis.

¹J. Li et al., *IEEE Trans. Magn.* **46**(6), 1475 (2010).

²A. Toba and T. A. Lipo, *IEEE Trans. Ind. Appl.* **36**(6), 1539 (2000).

³S. Mezani, K. Atallah, and D. Howe, *J. Appl. Phys.* **99**, 08R303 (2006).

⁴Z. P. Xia, Z. Q. Zhu, and D. Howe, *IEEE Trans. Magn.* **40**(4), 1864 (2004).

⁵Kyu-yun Hwang et al., *J. Appl. Phys.* **105**, 07F123 (2009).

⁶D. Zarko, D. Ban, and T. A. Lipo, *IEEE Trans. Magn.* **42**(7), 1828 (2006).